Impact of TIEG1 on the structural properties of fast- and slow-twitch skeletal muscle

Malek Kammoun, William Même, Sandra Même, Malayannam Subramaniam, John Hawse, Francis Canon, Sabine Bensamoun

Published in final edited form as:

Muscle Nerve. 2017 March ; 55(3): 410–416. doi:10.1002/mus.25252.

Impact of TIEG1 on the structural properties of fast and slow twitch skeletal muscle

Malek Kammoun, PhD[1], **Sandra Même, PhD**[2], **William Même, PhD**[2], **Malayannan Subramaniam, PhD**[3], **John R. Hawse, PhD**[3], **Francis Canon, PhD**[1], and **Sabine F. Bensamoun, PhD**[1]

[1]Sorbonne University, Université de technologie de Compiègne CNRS, UMR 7338 Biomechanics and Bioengineering, Centre de Recherches de Royallieu, Compiègne, France

[2]Centre de Biophysique Moléculaire, CNRS UPR4301, Orléans, France

[3]Department of Biochemistry and Molecular Biology, Mayo Clinic, 200 First Street SW, Rochester, MN 55905, USA

Abstract

Introduction—TIEG1 is a transcription factor that is highly expressed in skeletal muscle. The purpose of this study was to characterize the structural properties of both fast- (EDL) and slow- (soleus) twitch muscles in the hind-limb of TIEG1 deficient (TIEG$^{-/-}$) mice.

Methods—Ten slow and 10 fast muscles were analyzed from TIEG1$^{-/-}$ and WT mice using MRI texture (MRI-TA) and histological analyses.

Results—MRI-TA could discriminate between WT slow and fast muscles. Deletion of the TIEG1 gene led to changes in the texture profile within both muscle types. Specifically, muscle isolated from TIEG1$^{-/-}$ mice displayed hypertrophy, hyperplasia, and a modification of fiber area distribution.

Discussion—We demonstrate that TIEG1 plays an important role in the structural properties of skeletal muscle. This study further implicates important roles for TIEG1 in the development of skeletal muscle and suggests that defects in TIEG1 expression and/or function may be associated with muscle disease.

Keywords

Slow and fast muscles; magnetic resonance imaging; TIEG1; structural properties

INTRODUCTION

The transforming growth factor beta (TGF-β) inducible early gene-1 (TIEG1) is a member of the Krüppel-like family of transcription factors (KLF10) which has previously been

Correspondence to: Dr Sabine Bensamoun, PhD, Université de Technologie de Compiègne (UTC), Centre de Recherches de Royallieu, Laboratoire de Biomécanique et de BioIngénierie (BMBI), UMR CNRS 6600, BP 20529, 60205 Compiègne Cedex, France, Tel: (33) 03 44 23 43 90, sabine.bensamoun@utc.fr.

Financial Disclosures and Conflicts of Interest: None

shown to be expressed in multiple tissue types and cell lines[1–6]. TIEG1 has emerged as a key factor with regard to mediating TGF-β signaling[7–9]. Specifically, it is known to inhibit Smad7, a negative regulator of the TGFβ pathway, and induce Smad2 expression leading to enhancement of TGFβ signaling[10,11]. Overexpression of TIEG1 in multiple cell types is known to mimic TGFβ actions by inhibiting cell proliferation and inducing apoptosis in multiple cell types[12,3,4].

Previously, it has been shown that TIEG1 plays an important role in the growth, morphology, and mechanical properties of bone[13] and tendon[14]. Mechanical testing of these tissues (stretch, 3-point bending) in TIEG1−/− mice have revealed multiple defects and reduced strength[15–17]. Moreover, lack of TIEG1 expression induces morphological changes in these tissues, such as increased tendon-fiber diameter and reduced cortical- and cancellous-bone thickness. Based on these findings, and the fact that TIEG1 is most highly expressed in skeletal muscle[5], we sought to analyze the effects of TIEG1 on the morphological and structural properties of muscle.

The role of TIEG1 has been investigated in cardiac muscle[18] and myoblasts (C2C12)[19]. Interestingly, it has been shown that inhibition of TIEG1 induces cardiac-muscle hypertrophy accompanied by myofibrillar disarray and fibrosis[18]. These results suggest an important role for TIEG1 in normal cardiac development and function[18]. Concerning myoblast C2C12 cells, myostatin and TGF-β induce expression of TIEG1 mRNA[20]. These data suggest that TIEG1 regulates skeletal-muscle development, growth, and regeneration[20,19].

Several imaging techniques, including magnetic resonance imaging (MRI), ultrasound, and microscopy have allowed characterization of morphological and structural properties of tissues. These tools provide different fields of view of the sample at different resolutions. Microscopic techniques (optical, electronic, environmental, and fluorescent) have remained the methods utilized to characterize tissue composition. However, animals must be sacrificed, and non-invasive techniques, such as MRI, have begun to be used for *in vivo* analysis.

MRI acquisition requires a high magnitude field (7T or 9.4T) to characterize muscle metabolism[21], structure[22], and function[23] in mice. Specific MRI sequences, such as the transverse relaxation-time constant (T2), are also performed to detect muscle damage[21]. In addition to T2 analysis, quantitative texture analysis can reveal subtle structural changes to tissues that are not visible in MRI images. Those changes can be associated with, for example, the loss of cellular density (neurons), gliosis, inflammation (with edema) or, in contrast, fibrosis formation[24,25]. Analysis of texture has been applied successfully to liver[26], bone[27], muscle[22], and cerebral[24,28,25] tissues in humans and animals. This method can be used to compare and distinguish healthy from pathological tissues, to follow the development of pathology, or to study the efficacy of a therapeutic treatment.

The aim of this study was to characterize the impact of TIEG1 on the morphological and structural properties of fast and slow twitch skeletal muscles using MRI (with a texture analysis method) and histological techniques.

MATERIALS AND METHODS

TIEG1$^{-/-}$ mice

For this study, we utilized congenic C57BL/6 TIEG1 global knockout mice (female, aged 3 months) that were previously developed and characterized[13]. QRT-PCR was conducted on soleus and EDL muscles and confirmed that there is no expression of TIEG1 mRNA in these muscles. In addition Western Blotting was performed to validate the loss of TIEG1 protein expression (Fig. 1). We chose to analyze 3 month old female mice, since we have previously reported significant bone[17] and tendon phenotypes[15] in animals of this gender and age. The quadriceps muscle was dissected from a 3 month old female WT and TIEG1 KO mouse and rinsed in cold 1X PBS to remove blood contamination. Approximately 100 mg of tissue was homogenized in NETN buffer (150 mM NaCl, 1 mM EDTA, 20 mM Tris [pH 8.0], 0.5% Nonidet P-40), and insoluble material was pelleted. Protein concentrations were determined using Bradford Reagent, and 80 μg of muscle tissue lysate was separated using 7.5% SDS-PAGE. Proteins were transferred to PVDF membranes and probed with primary antibodies (TIEG1: Santa Cruz, clone A16; GAPDH: Millipore, clone 6C5; αTubulin: Sigma, clone DM1A) diluted in 5% non-fat dry milk in TBST overnight at 4°C on a rocking platform. Antibody dilutions were as follows: TIEG1, 1:500; GAPDH:,1:4000; and αTubulin, 1:100000. Anti-rabbit or anti-mouse HRP conjugated secondary antibodies were diluted at 1:2000 in 5% non-fat dry milk in TBST for 1 hour at room temperature. Membranes were visualized using enhanced chemiluminescence (Amersham Biosciences, Piscataway, NJ) and detected on a Licor imaging station.

The mice were housed at 22 ± 2°C in a humidity-controlled room, with a 12-h light/dark cycle in a center for breeding and distributing transgenic and mutant mice (CDTA: Cryopreservation, Distribution, Typage and Archivage animal, Orléans, France). They were fed standard laboratory chow *ad libitum*.

MRI tests

Selection of skeletal muscles—Two muscles known to have different fiber types were selected, namely the soleus (Sol) and the extensor digitorum longus (EDL) muscles. The soleus is a slow oxidative muscle and the EDL is a fast glycolytic muscle[29,30]. MRI experiments were performed on female TIEG1$^{-/-}$ (n=10) and WT control (n=10) mice, aged 3 months.

MRI acquisition—MRI was performed on a 9.4T horizontal ultra-shielded superconducting magnet dedicated to small-animal imaging (94/20 USR Bruker Biospec, Wissembourg, France) equipped with a 950mT/m gradient set. A loop gap coil (10 mm inner diameter) was used for both H transmission and reception. Axial images of the TIEG1$^{-/-}$ and WT hind-limb muscles were obtained using a gradient echo (Flash) sequence with the following parameters: TE/TR = 6 ms/252 ms, flip angle=20°, FOV size = 2×2cm, matrix size = 256 × 256, bandwidth= 50 kHz, slice thickness = 570μm, to display 78×78 μm^2 in plane resolution for a duration of 1 min (1 accumulation).

Mice were anesthetized during the MRI experiment with 1.5% isoflurane and a mixture of O_2/air (1:1) at an output of 0.7 L/min. Respiration was monitored during the experiment, and body temperature was maintained at 37°C using a warm-water circulation system.

Texture analysis—Acquired MR images were transferred to an external computer for data processing. Regions of interest (ROIs) were manually drawn within the soleus and EDL (Fig. 2). They were subsequently analyzed using Mazda software[31] (Mazda 4.6, MRI analysis software, ©1998–2007 by P.M.Szczypinski), which includes several texture-analysis methods. In this study, grey-level histograms, composed of different parameters, mean, standard devation, skewness, kurtosis, and different percentiles were used (Table 1). In addition, a co-occurrence matrix based on the following parameters: contrast, correlation, entropy, homogeneity, and energy was applied. This latter method consisted of selecting patterns on the images that were formed by 1 or several pixels and were in a particular direction. Moreover, the order of the methods corresponded to the length of the patterns formed by 2 pixels and 0° from the horizontal axis.

Data analyses—PCAs (principal-component analyses) were performed to identify the most significant texture parameters able to discriminate TIEG$^{-/-}$ muscle from WT muscle with a confidence level of 0.95. A 2-class (CI, CII) HAC (hierarchical ascending classification) was performed with the most discriminant texture parameters to differentiate the types of muscle (Sol *vs* EDL) and the muscle's genotype (TIEG$^{-/-}$ *vs*. WT). This presentation allowed us to distinguish the proportions of true negative (TN) and true positive (TP) values. As a consequence, the global value (Gv) corresponding to the number of well-classified muscles could be calculated: Gv = (TN + TP)/(total number of muscles).

Histological analysis

The same muscles (Sol, EDL) used in the MRI analysis were collected from TIEG1$^{-/-}$ (n=5) and WT (n=5) mice. The muscles were harvested, weighed, and immediately frozen in an isopentane bath which was cooled by liquid nitrogen to −80°C for histological analysis.

Two sections, 10 μm thick, were cut perpendicular to the muscle using a Microm HM 500M cryotome, at −20°C[32]. All sections were stained with azorubine to define the histological architecture of the muscle. Two regions within each section were then visualized under a Leica microscope using a 20× objective, and high-resolution images were acquired with an Olympus cooled digital camera DP-72. The fiber diameter and fiber cross-sectional area were determined using Image-Pro Premier 3D (v9.1 64-bit) Media Cybernetics software. In addition, the whole muscle area and mean number of fibers within the muscles were determined using Image J 1.43u software.

Statistical analysis

Statistical differences in muscle-fiber cross-sectional areas between TIEG1$^{-/-}$ and WT controls were assessed using the Student unpaired t-test (XLSTAT Software). Data are expressed as mean ± standard error of the mean (SEM). The level of statistical significance was fixed at P<0.05.

RESULTS

Correspondence factorial analyses (CFA) according to genotype (TIEG1$^{-/-}$ *vs*. WT)

Figure 2 shows the MRI images acquired for the WT and TIEG1$^{-/-}$, and recorded in the same area of the hind-limb. The comparison of both images revealed similar aspects of the cross sections. However, figure 3 illustrates the results from CFA for the Sol muscles and shows 2 distinct groups of texture profiles as a function of the genotype. Figure 4 shows a dendrogram representation of the HAC for the genotype effect in Sol (Fig. 4A) and EDL (Fig. 4B). Figure 4A shows that class I (CI) has a majority of WT Sol muscles (n=6) compared to class II (CII), which has the most TIEG1$^{-/-}$ Sol muscles (n=7). These results demonstrate the different texture profiles between WT and TIEG1$^{-/-}$ Sol muscles.

Similar HAC results were obtained for the EDL; Fig. 5B shows that CI gathered the most TIEG1$^{-/-}$ EDL muscles (n=6), whereas CII had more WT EDL muscles (n=5). The HAC EDL results indicate different texture behaviors between WT and TIEG1$^{-/-}$ muscles. The global values for the Sol and EDL were 76% (WT *vs* TIEG1$^{-/-}$) and 70%, (WT *vs* TIEG1$^{-/-}$), respectively.

CFA in function of the muscle type (Sol *vs.* EDL)

Figure 5 shows the CFA results for the WT Sol and EDL muscles. Two distinct groups (Sol *vs* EDL) can be identified. This result clearly shows the different textural properties of these WT muscles. The same difference was obtained in TIEG$^{-/-}$ Sol and EDL muscles. The global values obtained for the WT (Sol *vs* EDL) and TIEG1$^{-/-}$ (Sol *vs* EDL) muscles were 75% and 65%, respectively.

Histological analysis

The weights of the TIEG1$^{-/-}$ Sol (7.8 mg ± 0.6) and EDL (8.3 mg ± 0.4) muscles were significantly greater ($P < 0.01$) than the WT Sol (6.3 mg ± 0.7) and EDL (6.8 mg ± 0.4).

The results from azorubine staining show larger muscle fibers in both the Sol and EDL muscles in TIEG1$^{-/-}$ mice (Fig. 6A,C) compared to WT controls (Fig. 6B,D). This observation was compounded by the significantly higher (P<0.01; by ~40%) mean fiber area obtained for the Sol and EDL TIEG1$^{-/-}$ muscles compared to the WT controls (Fig. 7).

More specifically, EDL fiber-muscle area distribution (Fig. 8) varied between the 2 genotypes. TIEG1$^{-/-}$ EDL muscle had a different fiber area that was divided uniformly from 2500 μm^2 to 9500 μm^2, whereas WT EDL muscle was composed of 66% fiber areas that ranged from 1500 μm^2 to 3500 μm^2.

With regard to the Sol spectra, TIEG1$^{-/-}$ fiber area distribution resembled a Gaussian bell curve (Fig. 8) whereas 63% of the WT Sol fibers had their area within the 4500 μm^2 – 6000 μm^2 range, and 29% were within the 1500 μm^2 – 3000 μm^2 range.

In addition to fiber area, the Sol and EDL TIEG1$^{-/-}$ muscles had significantly (P<0.01) higher numbers of muscle fibers. The TIEG1$^{-/-}$ Sol had 856 (±48) fibers compared to 651 (±79) fibers for the WT Sol. The same trend was shown for the TIEG1$^{-/-}$ EDL, with 906

(±50) fibers compared to 754 (±29) for the WT littermates. It can be noted that, whatever the genotype, EDL had more muscle fibers compared to the Sol muscle. In addition, all the Sol and EDL TIEG1$^{-/-}$ muscle areas were significantly greater than those of the WT muscles. The TIEG1$^{-/-}$ Sol muscle area was equal to 1.68 mm^2 (±0.19) compared to 1.19 mm^2 (±0.06) for the WT Sol muscle. The EDL TIEG1$^{-/-}$ muscle area was 1.55 mm^2 (±0.11) compared to 0.99 mm^2 (±0.03) for EDT in WT mice.

DISCUSSION

The effect of the TIEG1 gene on muscle structure was investigated at a macroscopic level (muscle tissue) through MRI texture analysis (MRI-TA) and at the microscopic level (muscle fiber) through histological muscle fiber analysis.

MRI has the advantage that it can provide a complete representation of all the different muscles within the hind-limb, and these can be characterized simultaneously using specific MRI sequences. Although this technique is expensive, it enables one to keep the animal models alive and track changes in the same animals over time. In the literature, a few studies have applied the MRI-TA technique to detect changes in mouse muscle tissues[21,23] and brain[25]. This study characterized oxidative (Sol: slow-muscle fiber, type I) and glycolytic (EDL: fast-muscle fiber, type II) muscles[33] using MRI-TA technique. The high global value (an index used to assess the quality of the method) demonstrated the capability of this technique and the reliability of the data to characterize the textural profiles of different types of muscles.

The originality of this study was to use MRI-TA to characterize the texture profile of oxidative (Sol) and glycolytic (EDL) muscles in TIEG1$^{-/-}$ mice. Interestingly, even though there was deletion of the TIEG1 gene, the different texture behaviors observed between both wild type muscles were also identified between TIEG1$^{-/-}$ Sol and TIEG1$^{-/-}$ EDL muscles. Moreover, the CFA revealed that inhibiting TIEG1 expression affected the muscle-texture profile, regardless of muscle type (oxidative or glycolytic). It can be concluded that loss of TIEG1 expression alters the textural properties of skeletal muscles.

At the microscopic level, histological analyses revealed that deletion of TIEG1 caused hypertrophy of muscle fibers. TIEG1 has previously been shown to mediate growth factor and cytokine signaling in other tissues[34,35,10]. Myostatin is also a cytokine known to regulate the development, weight, and morphology of skeletal muscle[36], and it is possible that TIEG1 also plays a role in mediating the downstream effects of this important muscle cytokine. Such a possibility is worthy of future study and could explain some of the differences between WT and TIEG1$^{-/-}$ mice reported here. In addition to hypertrophy, hyperplasia was also observed as indicated by increased numbers of Sol and EDL TIEG1$^{-/-}$ muscle fibers. Hypertrophy was also observed by Bensamoun et al.[15] for TIEG1$^{-/-}$ tail tendons and by Rajamannan et al.[18] for TIEG1$^{-/-}$ heart tissues. In addition to these modifications, lack of TIEG1 expression also induced changes in the distribution of fiber areas compared to their WT littermates. Moreover, this distribution also differed according to muscle type: TIEG1$^{-/-}$ EDL had the same small, medium, or large fiber areas, whereas TIEG1$^{-/-}$ Sol fibers showed a Gaussian bell-curve distribution. The microscopic

modifications seen at the fiber level may be explained by the effect of TIEG1 at a cellular level (myoblast). Indeed, it has been shown that TIEG1 is a negative regulator within the myoblast pool and causes inhibition of myotube formation during myogenic differentiation[19]. These muscle modifications, shown at macroscopic and microscopic levels, were obtained in adult mice (3 months), an age at which alterations in the morphological properties of bone[17] and tendon[15] tissues have also been observed.

In conclusion, this report implicates an important role for TIEG1 in regulating the structural properties of skeletal muscle as has been previously shown for tendon[15] and bone[17]. Given the intimate interplay between bone and muscle, and possibly tendon, one could speculate that the differences in muscle observed here could be in part due to the known defects in the bones and tendons of these animals. Future studies utilizing Cre-mediated deletion of TIEG1 in tendon, bone, or muscle are warranted and will be helpful with regard to addressing this possibility. Based on our imaging and histological results, the MRI-TA technique might be useful for the study of diseased or pathological muscle conditions such as atrophy, dystrophy, and amyotrophy. In addition, future studies will focus on other MRI experiments, such as diffusion tensor imaging, to characterize muscle-fiber orientation in TIEG1$^{-/-}$ mice. Given the previous implications of TIEG1 in different diseases including osteoporosis, breast cancer[34] and cardiac hypertrophy[18], this study provides evidence that alterations in TIEG1 expression and/or function may also impact skeletal muscle development and may be associated with muscle disease. These areas merit further exploration.

Acknowledgments

The authors would like to thank the Picardie region, the European Regional Development Fund (ERDF) 2014/2020 and the National Institutes of Health grant: DE14036 (JRH and MS) for funding this work.

ABBREVIATIONS

EDL	extensor digitorum longus
HAC	Hierarchical Ascending Classification
MRI-TA	magnetic-resonance imaging –texture analyses
Sol	soleus
TGF-β	transforming growth factor β
TIEG1	transforming growth factor β inducible early gene-1
WT	wild-type
PBS	Phosphate Buffered Saline
EDTA	Ethylenediaminetetraacetic acid
PVDF	Polyvinylidene difluoride
GADPH	Glycéraldéhyde-3-phosphate déshydrogénase

TBST Tris-Buffered Saline and Tween

HRP Horseradish Peroxidase

References

1. Blok LJ, Grossmann ME, Perry JE, Tindall DJ. Characterization of an early growth-response gene, which encodes a zinc-finger transcription factor, potentially involved in cell-cycle regulation. Molecular Endocrinology. 1995; 9(11):1610–1620. [PubMed: 8584037]
2. Chalaux E, Lopez-Rovira T, Rosa JL, Pons G, Boxer LM, Bartrons R, et al. A zinc-finger transcription factor induced by TGF-beta promotes apoptotic cell death in epithelial Mv1Lu cells. Febs Letters. 1999; 457(3):478–482. [PubMed: 10471833]
3. Hefferan TE, Reinholz GG, Rickard DJ, Johnsen SA, Waters KM, Subramaniam M, et al. Overexpression of a nuclear protein, TIEG, mimics transforming growth factor-beta action in human osteoblast cells. The Journal of biological chemistry. 2000; 275(27):20255–20259. [PubMed: 10816551]
4. Ribeiro A, Bronk SF, Roberts PJ, Urrutia R, Gores GJ. The transforming growth factor beta(1)-inducible transcription factor, TIEG1, mediates apoptosis through oxidative stress. Hepatology. 1999; 30(6):1490–1497. [PubMed: 10573529]
5. Subramaniam M, Harris SA, Oursler MJ, Rasmussen K, Riggs BL, Spelsberg TC. Identification of a novel TGF-beta-regulated gene encoding a putative zinc finger protein in human osteoblasts. Nucleic acids research. 1995; 23(23):4907–4912. [PubMed: 8532536]
6. Tau KR, Hefferan TE, Waters KM, Robinson JA, Subramaniam M, Riggs BL, et al. Estrogen regulation of a transforming growth factor-beta inducible early gene that inhibits deoxyribonucleic acid synthesis in human osteoblasts. Endocrinology. 1998; 139(3):1346–1353. [PubMed: 9492071]
7. Hsu TH, Xiao JL, Tsao YW, Kao YL, Huang SH, Liao WY, et al. Analysis of the paracrine loop between cancer cells and fibroblasts using a microfluidic chip. Lab on a chip. 2011; 11(10):1808–1814. [PubMed: 21491053]
8. Subramaniam M, Hawse JR, Bruinsma ES, Grygo SB, Cicek M, Oursler MJ, et al. TGFbeta inducible early gene-1 directly binds to, and represses, the OPG promoter in osteoblasts. Biochemical and biophysical research communications. 2010; 392(1):72–76. [PubMed: 20059964]
9. Wu MJ, Wu WC, Chang HW, Lai YT, Lin CH, Yu WC, et al. KLF10 affects pancreatic function via the SEI-1/p21Cip1 pathway. The international journal of biochemistry & cell biology. 2015; 60:53–59. [PubMed: 25578559]
10. Johnsen SA, Subramaniam M, Janknecht R, Spelsberg TC. TGFbeta inducible early gene enhances TGFbeta/Smad-dependent transcriptional responses. Oncogene. 2002; 21(37):5783–5790. [PubMed: 12173049]
11. Johnsen SA, Subramaniam M, Katagiri T, Janknecht R, Spelsberg TC. Transcriptional regulation of Smad2 is required for enhancement of TGFbeta/Smad signaling by TGFbeta inducible early gene. Journal of cellular biochemistry. 2002; 87(2):233–241. [PubMed: 12244575]
12. Tachibana I, Imoto M, Adjei PN, Gores GJ, Subramaniam M, Spelsberg TC, et al. Overexpression of the TGFbeta-regulated zinc finger encoding gene, TIEG, induces apoptosis in pancreatic epithelial cells. The Journal of clinical investigation. 1997; 99(10):2365–2374. [PubMed: 9153278]
13. Subramaniam M, Gorny G, Johnsen SA, Monroe DG, Evans GL, Fraser DG, et al. TIEG1 null mouse-derived osteoblasts are defective in mineralization and in support of osteoclast differentiation in vitro. Molecular and cellular biology. 2005; 25(3):1191–1199. [PubMed: 15657444]
14. Gumez L, Bensamoun SF, Doucet J, Haddad O, Hawse JR, Subramaniam M, et al. Molecular structure of tail tendon fibers in TIEG1 knockout mice using synchrotron diffraction technology. Journal of applied physiology (Bethesda, Md: 1985). 2010; 108(6):1706–1710.
15. Bensamoun SF, Tsubone T, Subramaniam M, Hawse JR, Boumediene E, Spelsberg TC, et al. Age-dependent changes in the mechanical properties of tail tendons in TGF-beta inducible early gene-1 knockout mice. Journal of applied physiology (Bethesda, Md : 1985). 2006; 101(5):1419–1424.

16. Hawse JR, Cicek M, Grygo SB, Bruinsma ES, Rajamannan NM, van Wijnen AJ, et al. TIEG1/KLF10 modulates Runx2 expression and activity in osteoblasts. PloS one. 2011; 6(4):e19429. [PubMed: 21559363]
17. Bensamoun SF, Hawse JR, Subramaniam M, Ilharreborde B, Bassillais A, Benhamou CL, et al. TGFbeta inducible early gene-1 knockout mice display defects in bone strength and microarchitecture. Bone. 2006; 39(6):1244–1251. [PubMed: 16876494]
18. Rajamannan NM, Subramaniam M, Abraham TP, Vasile VC, Ackerman MJ, Monroe DG, et al. TGFbeta inducible early gene-1 (TIEG1) and cardiac hypertrophy: Discovery and characterization of a novel signaling pathway. Journal of cellular biochemistry. 2007; 100(2):315–325. [PubMed: 16888812]
19. Miyake M, Hayashi S, Iwasaki S, Chao G, Takahashi H, Watanabe K, et al. Possible role of TIEG1 as a feedback regulator of myostatin and TGF-beta in myoblasts. Biochemical and biophysical research communications. 2010; 393(4):762–766. [PubMed: 20171187]
20. Miyake M, Hayashi S, Iwasaki S, Uchida T, Watanabe K, Ohwada S, et al. TIEG1 negatively controls the myoblast pool indispensable for fusion during myogenic differentiation of C2C12 cells. Journal of cellular physiology. 2011; 226(4):1128–1136. [PubMed: 20945337]
21. Martins-Bach AB, Malheiros J, Matot B, Martins PC, Almeida CF, Caldeira W, et al. Quantitative T2 combined with texture analysis of nuclear magnetic resonance images identify different degrees of muscle involvement in three mouse models of muscle dystrophy: mdx, Largemyd and mdx/Largemyd. PloS one. 2015; 10(2):e0117835. [PubMed: 25710816]
22. Herlidou S, Rolland Y, Bansard JY, Le Rumeur E, de Certaines JD. Comparison of automated and visual texture analysis in MRI: characterization of normal and diseased skeletal muscle. Magnetic resonance imaging. 1999; 17(9):1393–1397. [PubMed: 10576724]
23. Mathur S, Vohra RS, Germain SA, Forbes S, Bryant ND, Vandenborne K, et al. Changes in muscle T2 and tissue damage after downhill running in mdx Mice. Muscle & Nerve. 2011; 43(6):878–886. [PubMed: 21488051]
24. Calas AG, Richard O, Meme S, Beloeil JC, Doan BT, Gefflaut T, et al. Chronic exposure to glufosinate-ammonium induces spatial memory impairments, hippocampal MRI modifications and glutamine synthetase activation in mice. Neurotoxicology. 2008; 29(4):740–747. [PubMed: 18562008]
25. Meme S, Calas AG, Montecot C, Richard O, Gautier H, Gefflaut T, et al. MRI characterization of structural mouse brain changes in response to chronic exposure to the glufosinate ammonium herbicide. Toxicological sciences: an official journal of the Society of Toxicology. 2009; 111(2):321–330. [PubMed: 19638430]
26. Jirak D, Dezortova M, Taimr P, Hajek M. Texture analysis of human liver. Journal of magnetic resonance imaging: JMRI. 2002; 15(1):68–74. [PubMed: 11793459]
27. Herlidou S, Grebe R, Grados F, Leuyer N, Fardellone P, Meyer ME. Influence of age and osteoporosis on calcaneus trabecular bone structure: a preliminary in vivo MRI study by quantitative texture analysis. Magnetic resonance imaging. 2004; 22(2):237–243. [PubMed: 15010116]
28. Herlidou-Meme S, Constans JM, Carsin B, Olivie D, Eliat PA, Nadal-Desbarats L, et al. MRI texture analysis on texture test objects, normal brain and intracranial tumors. Magnetic resonance imaging. 2003; 21(9):989–993. [PubMed: 14684201]
29. Agbulut O, Noirez P, Beaumont F, Butler-Browne G. Myosin heavy chain isoforms in postnatal muscle development of mice. Biology of the cell/under the auspices of the European Cell Biology Organization. 2003; 95(6):399–406.
30. Hamalainen N, Pette D. The histochemical profiles of fast fiber types IIB, IID, and IIA in skeletal muscles of mouse, rat, and rabbit. The journal of histochemistry and cytochemistry: official journal of the Histochemistry Society. 1993; 41(5):733–743. [PubMed: 8468455]
31. Szczypinski PM, Strzelecki M, Materka A, Klepaczko A. MaZda–a software package for image texture analysis. Computer methods and programs in biomedicine. 2009; 94(1):66–76. [PubMed: 18922598]

32. Kammoun M, Cassar-Malek I, Meunier B, Picard B. A simplified immunohistochemical classification of skeletal muscle fibres in mouse. European journal of histochemistry: EJH. 2014; 58(2):2254. [PubMed: 24998919]

33. Augusto V, Padovani CR, Campos GR. Skeletal muscle fiber types in C57BL6J mice. Braz J Morphol Sci. 2004; 21(2):89–94.

34. Subramaniam M, Hawse JR, Johnsen SA, Spelsberg TC. Role of TIEG1 in biological processes and disease states. Journal of cellular biochemistry. 2007; 102(3):539–548. [PubMed: 17729309]

35. Subramaniam M, Hefferan TE, Tau K, Peus D, Pittelkow M, Jalal S, et al. Tissue, cell type, and breast cancer stage-specific expression of a TGF-beta inducible early transcription factor gene. Journal of cellular biochemistry. 1998; 68(2):226–236. [PubMed: 9443078]

36. Wang Q, McPherron AC. Myostatin inhibition induces muscle fibre hypertrophy prior to satellite cell activation. The Journal of physiology. 2012; 590(9):2151–2165. [PubMed: 22393251]

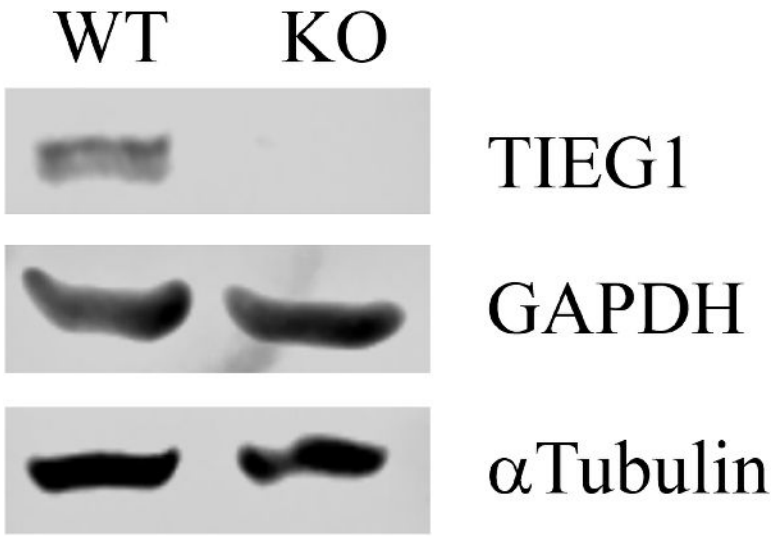

FIGURE 1.

TIEG1 protein expression in skeletal muscle. Western blot indicates TIEG1 protein levels in the skeletal muscle of wild-type (WT) and TIEG1 knockout (KO) mice. GAPDH/Tubulin was used as a loading control.

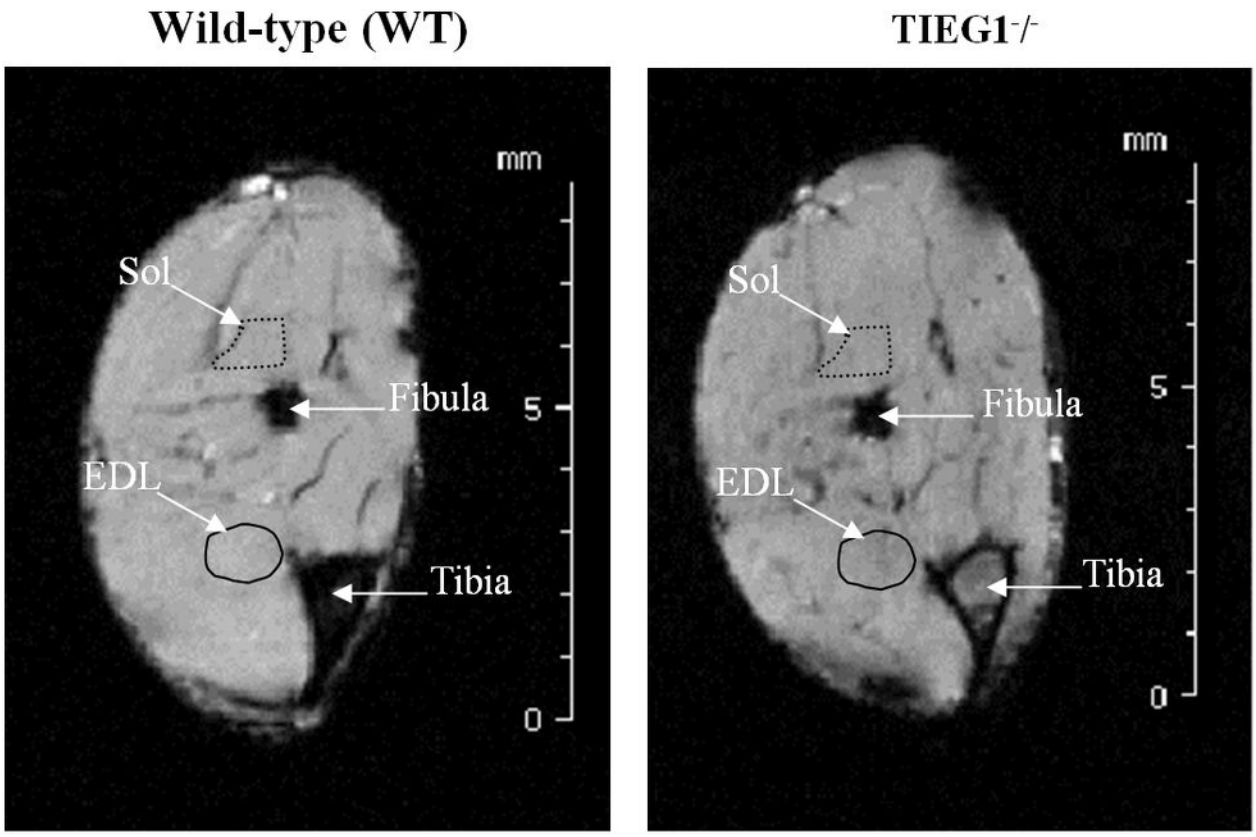

FIGURE 2.

MRI axial image of wild-type (WT) and TIEG1$^{-/-}$ hind limbs. Regions of interest (ROI) were manually placed within the soleus (Sol) and extensor digitorum longus (EDL) muscles.

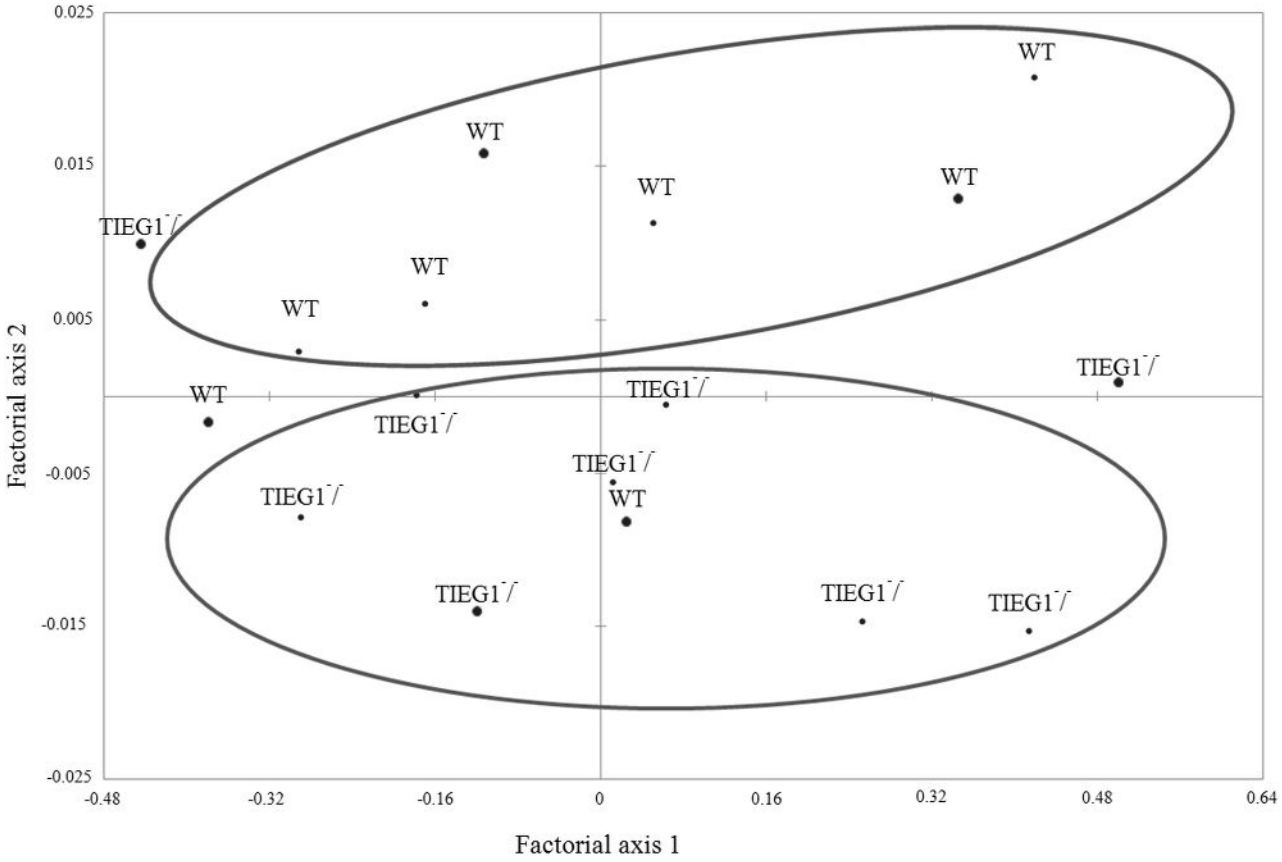

FIGURE 3.

Correspondence factorial analysis (CFA) of soleus ROIs according to genotype (wild type (WT) *vs* TIEG1$^{-/-}$). It can be noted that among the total number of Sol muscles (n=10 WT, n=10 TIEG1$^{-/-}$), 6 WT and 7 TIEG1$^{-/-}$ were well classified.

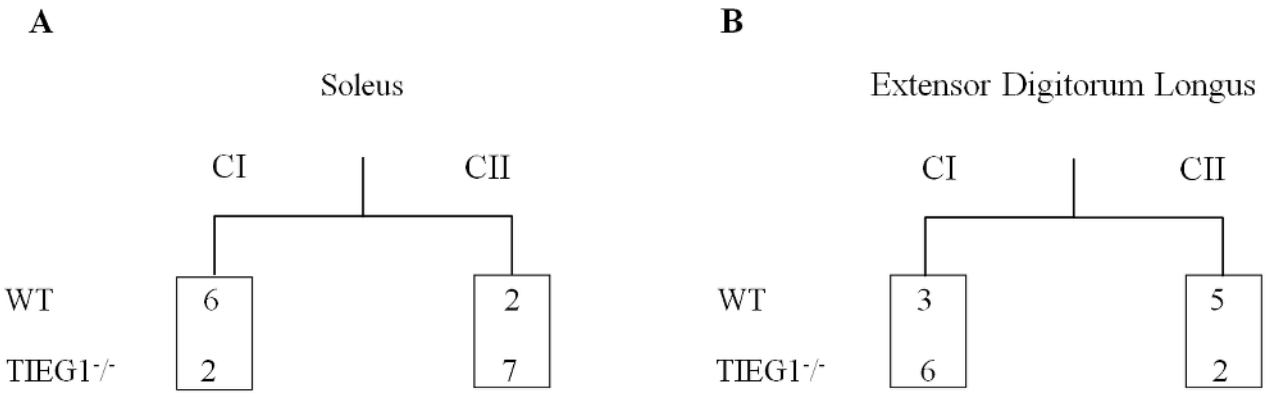

FIGURE 4.

Hierarchical ascending classifications (HAC) of the soleus (A) and extensor digitorum longus (B) according to function in wild-type (WT) *vs* TIEG1$^{-/-}$ mice.

CI: class I, CII: class II

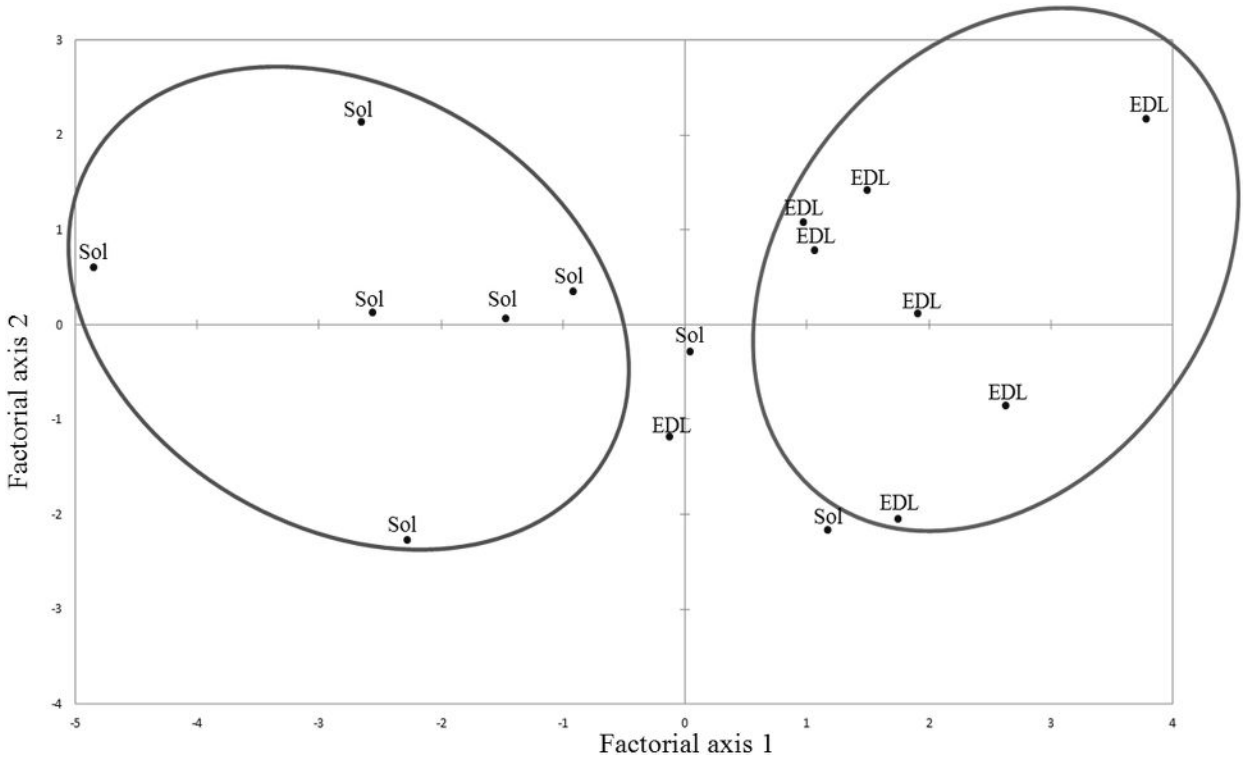

FIGURE 5.

Correspondence factorial analysis (CFA) of wild-type soleus (Sol) and extensor digitorum longus (EDL) regions of interests. It can be noted that among the total number of muscles (n=10 Sol, n=10 EDL), 6 Sol and 7 EDL were well classified.

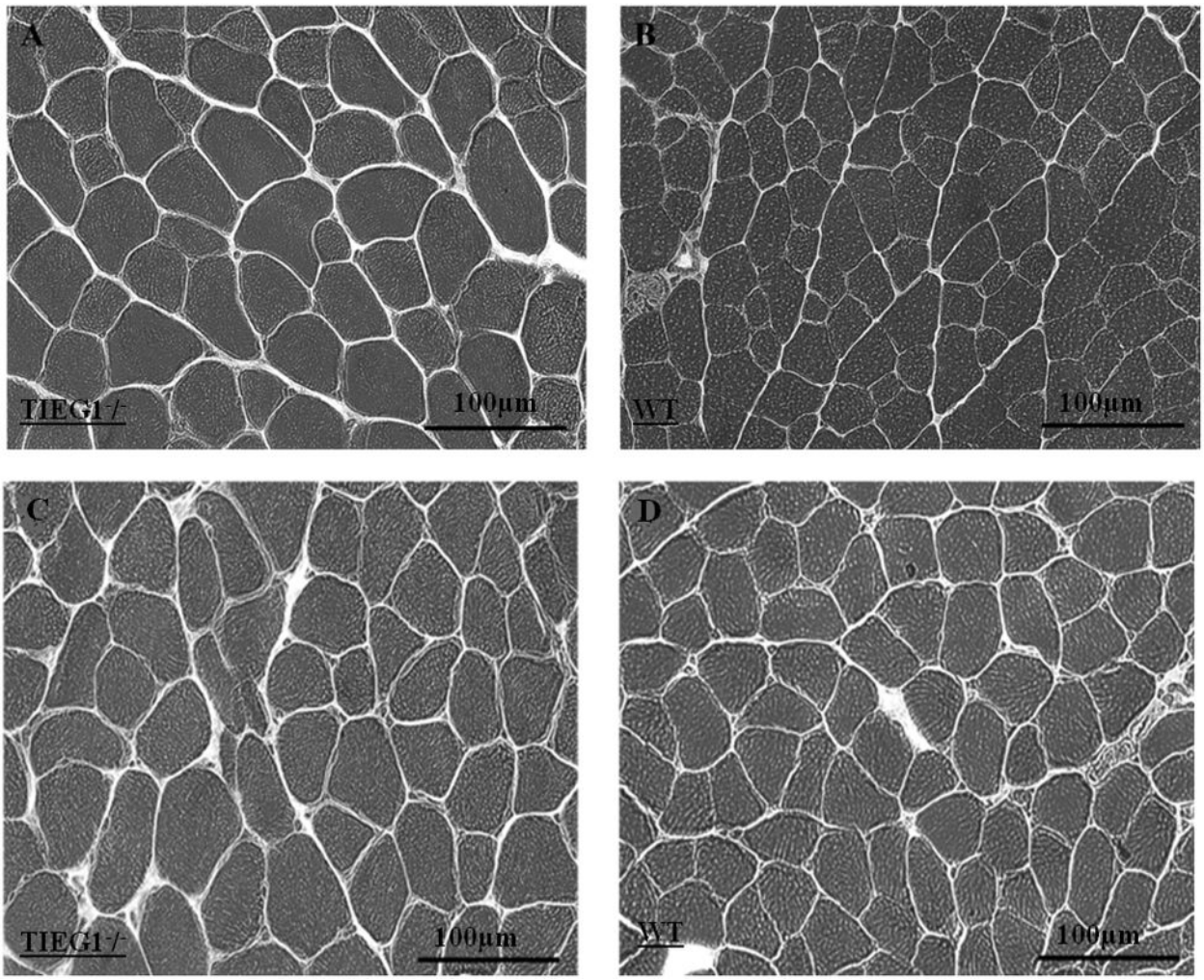

FIGURE 6.

Azorubine staining of an extensor digitorum longus muscle (TIEG1$^{-/-}$: A, wild-type: B) and soleus muscle (TIEG1$^{-/-}$: C, wild-type: D).

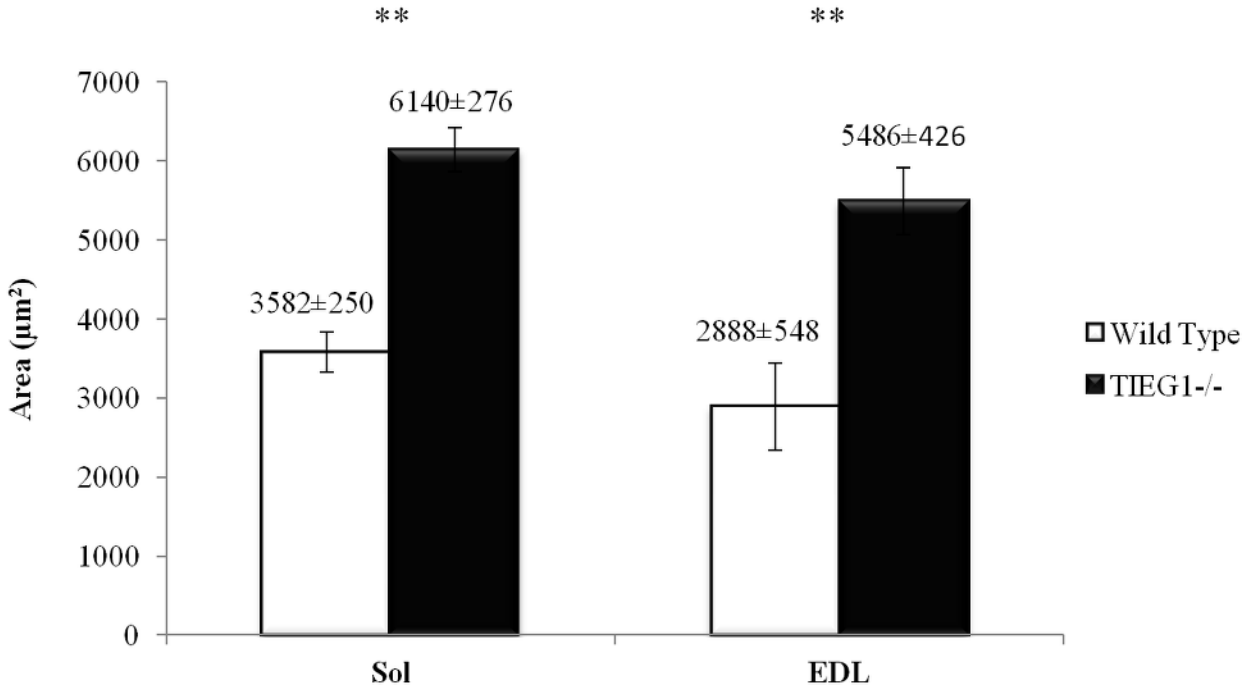

FIGURE 7.

Muscle-fiber areas (mean ± SEM) for wild type and TIEG1$^{-/-}$ soleus (Sol) and extensor digitorum longus (EDL) muscles. **: P<0.01

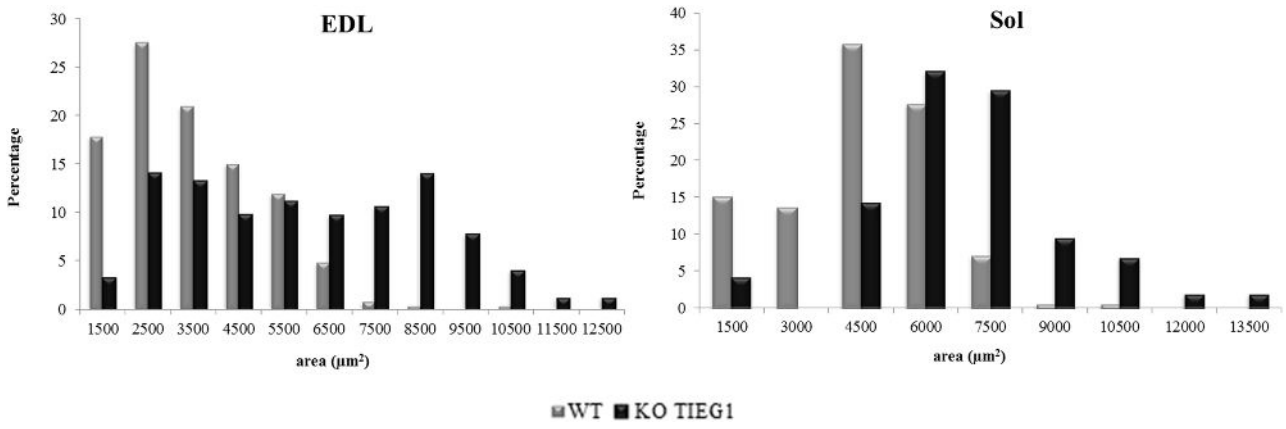

FIGURE 8.

Distribution of fiber area in the extensor digitorum longus (EDL) and soleus (Sol) muscles according to genotype (wild-type (WT) *vs* TIEG1$^{-/-}$).

TABLE 1

Summary of the texture analysis methods used and the parameters they provide.

Texture analysis methods	Available texture parameters
Gray level histogram	mean, standard deviation, skewness, kurtosis, percentiles 1%, 10%, 50%, 90%, 99%
Co-occurrence matrix (d=1, θ=0°)	Contrast correlation, entropy, homogeneity,energy